RESEARCH PAPER

Effect of manufacturing angle on surface characteristics and fibroblast adhesion of poly-caprolactone/hyaluronic acid scaffold for tissue engineering

***Nilofar Khodami Moghari*[1], *Azadeh Asefnejad*[1*]**

[1]*Department of Biomedical Engineering, Science and Research Branch, Islamic Azad University, Tehran, Iran*

ABSTRACT

Cell adhesion to surfaces plays a crucial role in tissue engineering and is influenced by surface characteristics and material properties. Hydrophilicity is an important property for scaffolds to facilitate cell adhesion and growth, but most synthetic polymers lack this property, unlike natural polymers such as gelatin, sodium alginate, and hyaluronic acid (HA). Therefore, the objective of this study is to investigate the impact of the manufacturing angle on the surface characteristics and fibroblast adhesion of a three-dimensional scaffold made of poly-caprolactone and HA. The scaffolds were produced using 3D printing with various angles (60-60°, 45-90°, and 30-30°) and subsequently coated with a solution containing HA, zinc nanoparticles (ZnO), and drugs. Mechanical and biological properties of the scaffolds, including swelling, biodegradability, biocompatibility, and cell viability, were evaluated, while the drug release rate was measured. Optical and scanning electron microscopes (SEM), energy-dispersive X-ray spectroscopy (EDAX), and mapping were employed to conduct morphological and elemental analyses. The findings demonstrate that the manufacturing angle significantly influences the scaffold's surface characteristics and fibroblast adhesion, and surface coating can improve the scaffold's properties for tissue engineering applications. The coated scaffolds exhibited higher swelling percentage, lower degradation percentage, and a drug release rate of 27% over 10 hours, while maintaining excellent biocompatibility with 102% cell coverage.

Keywords: *Surface characteristics, 3D scaffold, Poly-caprolactone, Hyaluronic acid*

How to cite this article

Khodami Moghari N, Asefnejad A. Effect of manufacturing angle on surface characteristics and fibroblast adhesion of poly-caprolactone/hyaluronic acid scaffold for tissue engineering. Nanomed J. 2025; 12(4): 768-788. DOI:10.22038/NMJ.2025.79671.1966

INTRODUCTION

Tissue engineering is a promising approach for repairing and regenerating damaged tissues in the human body [1]. Different types of materials, including autografts, allografts, xenografts, and synthetic materials, have been used in tissue engineering [2-3]. However, these types of grafts have limitations such as limited supply, inability to treat defects, and high failure rates [3-4]. 3D printing technology can be used to fabricate scaffolds with adjustable mechanical properties and porosity, which can improve cell growth and prevent tension in damaged tissues. Besides mechanical properties and porosity, an ideal scaffold should possess other important features such as biocompatibility, suitable surface, and biodegradability [5]. Natural materials are often preferred for tissue engineering due to their biological signals and mechanical properties [6]. Polymers are widely used in medicine, including constructing scaffolds for various tissue engineering applications. The design of polymer scaffolds plays a crucial role in proper cell growth, and the properties of biocompatibility, biodegradability, and mechanical strength must be considered [7]. Hyaluronic acid (HA) is a large molecule that possesses unique properties such as the ability to bind to water and form a gel-like consistency, store growth factors, and enhance cell adhesion and migration [8].

3D printing technology offers several advantages such as cost and time savings, reliability, and material diversity. It enables the precise fabrication of complex scaffolds by layering materials and can mix several types of materials to produce diverse sample. This research aims to design and fabricate 3D scaffolds using polycaprolactone (PCL) and HA through 3D printing technology, which offers several advantages for tissue engineering applications. The scaffolds may be designed with different angles to evaluate their physical, morphological, and biological properties

*Corresponding author(s) Email: asefnejad@srbiau.ac.ir.

Note. This manuscript was submitted on April 30, 2024; approved on September 15, 2024

using various tests. Soft tissue repair requires suitable alternative structures with biomimetic properties, and scaffold topography is crucial for cell adhesion. This study is innovative as it explores the combination of PCL and HA to produce a biomimetic tissue scaffold, which has not been studied before. Integrins, proteins present in the extracellular matrix (ECM), play a critical role in mediating cell adhesion and signaling. In laboratory conditions, cell patterning depends on creating an adhesive layer with controlled size and chemical properties. Various surfaces, including metals, polymers, ECM proteins, and promoter peptides, have been studied to control the selective adhesion of cells at the microscopic level. Additionally, the resistance of different surfaces to cell adhesion has been investigated [9-10]. Cell patterning methods typically involve selectively attaching cells to a pre-made adhesive or non-adhesive surface using conventional photochemical or soft lithography techniques. However, direct patterning methods allow for the direct placement of cells in specific locations without pre-patterning. Another direct patterning technique is matrix-assisted pulsed laser evaporation (MAPLE), which utilizes focused laser pulses to transfer cells through an optically transparent quartz substrate that is coated with a biopolymer containing the cells [11-14]. The cells are transferred to a receiving medium, typically a microscopic glass slide coated with a biopolymer that allows for cell adhesion and growth. Material transfer is accomplished by focusing the laser at the boundary between the transparent quartz substrate and the light-absorbing biological layer containing cells. The computer-controlled movement of the receiving substrate enables the formation of desired patterns [12]. PCL is a versatile and relatively inexpensive linear synthetic biodegradable aliphatic polyester that can transform into various forms, making it an attractive material for scaffold development in tissue engineering applications. PCL is an FDA-approved polyester with excellent thermal stability and is commonly used in medical applications due to its ease of processing. However, PCL's hydrophobic nature and sensitivity to surface changes may affect its properties, such as degradation and cellular attraction [15-18]. Therefore, PCL is often combined with natural polymers or functionalized using short chains of amino acids and peptide chains to increase its biocompatibility and promote adhesion, proliferation, and differentiation of seeded cells [19-22]. The ideal scaffold for tissue engineering should possess interconnected porous architecture, porosity, controlled degradation, sufficient mechanical strength, and biocompatibility. Recent advances in tissue engineering have led to the development of scaffolds with ideal properties using composites and blends, as the biocompatibility and slow degradation of synthetic polymers, including PCL, limit their use. The primary goal of this investigation is to construct a biomimetic scaffold that shows mechanical properties and biological behaviors appropriate and compatible with the growth of fibroblast cells. Furthermore, the study aims to fabricate and characterize a 3D scaffold using poly-caprolactone and HA through 3D printing technology, which can be utilized for various orthopedic fractures.

MATERIALS AND METHODS

In this work a prepared films of PCL with varying percentages of 5, 10, and 15% using chloroform solvent. After the solvent completely evaporated, the films were removed from the glass plate. We found that a 5% concentration was optimal for printing the PCL scaffold. Using a 3D printer (X BioFab4), the authors printed the scaffold with three different positioning angles. Figure 1 shows the fabricated film composed of 5% polycaprolactone (PCL). The image highlights the physical properties of the film, including its texture and uniformity, which are critical for assessing its suitability for various applications in tissue engineering. The concentration of 5% PCL is significant as it influences the mechanical strength and biocompatibility of the film, making it a vital component in the design of scaffolds for regenerative medicine. Figure 2 (a-c) presents images of printed scaffolds manufactured at various angles to investigate their structural properties. Figure 2 (a) shows the scaffold with an angle configuration of 0 × 60 × 60, while Figure 2 (b) features the configuration of 0 × 90 × 45, and Figure 2 (c) shows the 0 × 30 × 30 arrangement. These differing angles are essential for examining how scaffold orientation affects surface characteristics, mechanical stability, and cellular adhesion in tissue engineering applications. To improve the scaffold's surface properties, the authors coated it with a solution containing hydrophilic polymers, zinc nanoparticles (ZnO), and cloxacillin. The scaffold was immersed in the solution for 15 minutes and then dried in the oven. The authors printed the circular scaffold structures with a diameter of 2 cm and 5 layers using a 3D printer (X2 Biofab). Figure 3 (a) shows the solution used for coating the scaffolds, while Figure 3 (b) illustrates the stages of scaffold immersion. Despite advancements in direct patterning techniques like matrix-assisted pulsed laser evaporation (MAPLE) for cell transduction,

several research gaps remain. First, there is limited understanding of the long-term viability and functionality of cells after transfer, particularly regarding how different biopolymer compositions affect cellular behavior post-patterning.

Fig. 1. Fabricated film, 5% PCL

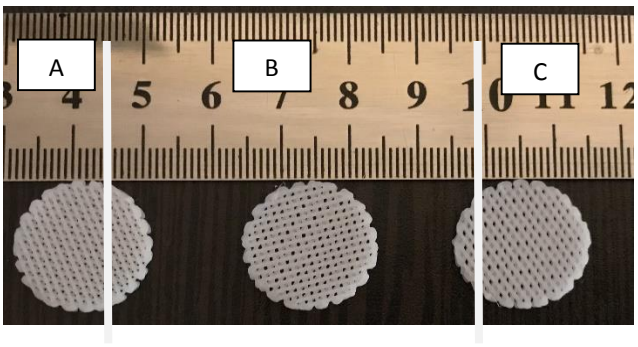

Fig. 2. The image of printed scaffolds with different angles, A) 0 × 60 × 60, B) 0 × 90 × 45, C) 0 × 30 × 30

a

b

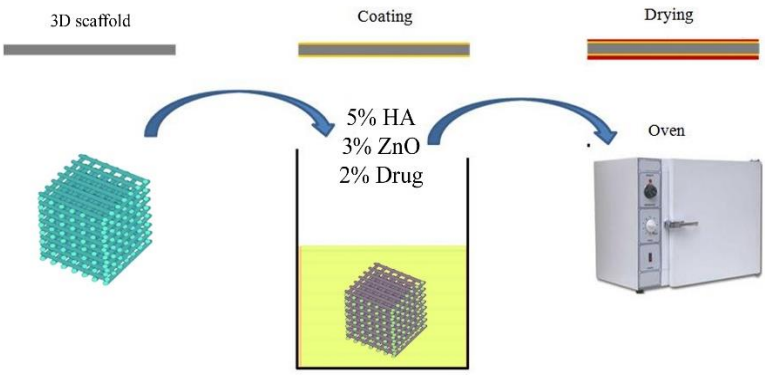

Fig. 3. Schematic of preparation of HA-ZnO-Drug

Additionally, the influence of varying laser parameters on cell integrity and pattern resolution requires further investigation. Lastly, the scalability of MAPLE for clinical applications, including its integration with existing tissue engineering methodologies, has not been thoroughly explored, showing the need for comprehensive studies to assess its practical utility in real-world scenarios.

The study utilized various essential equipment for the experiments, as detailed in Table 1. The C-MAG HS7 magnetic stirrer from IKA® was used for stirring solutions, while the STM-50 traction device from SANTAM facilitated mechanical testing. Imaging was conducted using an MP-bell optical microscope and a SEM. The controlled environment was ensured with the AIS2100 laboratory hood from SERONTECHNOLOGIES, and optimal growth conditions were maintained in an incubator. Precise measurements were taken using the MWMMERT – IPP55Plus scales from Germany. Table 2 shows the polycaprolactone (PCL) bioinks, including formulations with varying concentrations: 5 grams (A), 10 grams (B), and 15 grams (C) of PCL in 100 cc of chloroform. Table 3 describes the design of three-dimensional scaffolds, with the first scaffold (0×60×60A) consisting of 5 grams of PCL without additional components. The second and third scaffolds (45×90×0B and 0×30×30C) lack specific details, while an A/HA/ZnO formulation incorporates hyaluronic acid, zinc oxide, and a drug for enhanced properties. Finally, Table 4 shows the weight and atomic percentages of elements from energy-dispersive X-ray spectroscopy (EDS) analysis, providing insights into the scaffolds' elemental composition and biocompatibility, crucial for their effectiveness in tissue engineering applications.

Table 1. Equipment used in the experiments

Device name	Device brand	Device model
stirrer (magnetic stirrer)	IKA®	C-MAG HS7
Traction device	Santam	STM-50
optical microscope	Bell/Italy	MP-bell
Scanning Electron Microscope (SEM)		
Laboratory hood	SERONTECHNOLOGIES	AIS2100
Incubator	Equipping server	---
scales	Germany	MWMMERT – IPP55Plus

Table 2. Polycaprolactone bioink coding

Created solution code	Description	PCL
A	The solutions were prepared using a magnetic stirrer.	5 gr PCL in 100 cc Chloroform
B		10 gr PCL in 100 cc Chloroform
c		15 gr PCL in 100 cc Chloroform

Table 3. Design of three-dimensional scaffold

Description	Drug	ZnO	HA	PCL	
Temperature	---	---	---	5 gr PCL in 100 cc Chlorof	A=60×60×0
was not used in	---	---	---		B=0×90×45
any stage for	---	---	---		C=30×30×0
construction.	5 gr Drug in 100cc DW	3 gr ZnO in 100cc DW	5 gr HA in 100cc DW		A/HA/ZnO

Table 4. Weight and atomic percentage of elements in 3D scaffolds using EDS analysis

Elements	60-60		45-90		30-30	
	W%	A%	W%	A%	W%	A%
C	37.41	49.54	43.86	55.13	38.72	49.88
N	5.10	5.80	4.79	5.17	5.98	6.61
O	39.64	39.41	38.24	36.08	40.83	39.49
Cl	4.41	1.98	3.10	1.32	2.96	1.29
Zn	13.44	3.27	10.01	2.31	11.51	2.73
	100.00	100.00	100.00	100.00	100.00	100.00

Morphology observation

An optical microscope was used for the initial observation of the scaffolds and the morphology of the pores and strands. The optical microscope used is the MP-Bell model, which was used for 3D samples with and without cover. A scanning electron microscope (SEM) was used to evaluate the scaffolds and examine the surfaces. First, the samples were coated with gold, and then imaging was done and the diameter of the strands and the area of the coating particles on the scaffolds were measured by Image-J software. The scanning electron microscope used is the AIS2100 model, which was imaged for the samples with and without coating.

Element Identification Analysis (EDS)

It will be possible to identify the constituent elements of the sample in a semi-quantitative way. For EDS analysis, at least 5 mg of particle sample is required. The EDS test is calculated semi-quantitatively and the energy spectrum will also be presented. The EDS device used is the EVO®MA model, which was performed for the samples that were evaluated for bioactivity.

MAP analysis

In MAP analysis, it may be possible to present the frequency distribution of the elements in an image. Analysis has been done for the samples that were evaluated.

Mechanical testing

The tensile test is a destructive test used to subject a sample to a one-dimensional tensile force until it reaches the breaking point while recording elongation and applied force simultaneously. The test results are used for quality control purposes and to predict the material's reaction under other types of forces. The engineering stress-strain curve is drawn based on the applied force-elongation values, and the data obtained from this test are used to determine the material's mechanical properties, including yield stress, ultimate tensile strength (UTS), ductility, modulus of elasticity or Young's modulus, and toughness. The uniaxial tensile test is used for isotropic materials, while the biaxial test is used for anisotropic materials such as composites. The test involves applying a tensile force to the sample until it fails, and the force required to cause elongation is reported, and the force-elongation curve is plotted.

$$\sigma = P/A0 \qquad \text{Eq. 1}$$

$$e = L/L0 \qquad \text{Eq. 2}$$

The stress-strain curves, engineering stress (σ) represents the force divided by the initial cross-sectional area, while engineering strain (e) represents the increase in length divided by the initial gage length. These parameters are independent of the geometry and shape of the material [23-28]. The linear portion of the stress-strain curve up to the yielding point is called the elastic region, where stress and strain have a linear relationship, and Hooke's law is established as follows:

$$E = \sigma/e \qquad \text{Eq. 3}$$

The constant E in the equation above is known as the elastic modulus or Young's modulus, which is specific to each material. We evaluated the mechanical properties of the samples using a strength testing machine according to the ISO-6824 standard. The samples were attached to a 10 × 30 mm square paper frame [29-37] and subjected to a tensile strength test. The paper frame was placed between the jaws of the stretching machine, 3 cm apart, with an applied force of 10 N. The stretching speed was set at 5 mm/min, and the test was conducted at 30% humidity and 23 ± 2°C using an SMT-20 model device.

Inflation evaluation

In order to check the amount of water absorption on the coated and non-coated scaffolds, first cut the scaffolds to a certain size and weigh them, and then put them in a beaker filled with phosphate buffer saline (PBS) solution and weigh them again. To be place the obtained numbers in the following formula and get the percentage of inflation.

$$WRV = m3\text{-}m4/m4 \qquad \text{Eq. 4}$$

WRV is equal to the percentage of water absorption, m3 is the mass of the sample after swelling and m4 is the mass of the dry sample. Inflation was done for 120 minutes for samples with and without coating.

Biodegradability evaluation

Biodegradability test was used in order to check the level of stability and measure the rate of degradation in the external environment. For this purpose, the scaffold was first weighed (dry weight) and placed in phosphate buffered salt for 20 days. Every 24 hours, the samples were removed from the solution and dried with filter paper and the weight of the sample was measured. The authors conducted the in vitro cell culture test in accordance with the ISO10993-5 standard to evaluate the cultivation of fibroblast cells on nanoscaffolds. To prepare one-day extracts, a 3 square centimeter sample was placed inside a sterile microtube, and 1 milliliter of RPMI culture medium without FBS was added. The sample was then incubated at 5% carbon dioxide gas, 90% humidity, and 37°C. The MTT test with a concentration of 0.5 mg/ml was used to assess toxicity. For this, 5000 L929 cells in 100 microliters of culture medium (RPMI) containing serum were added to three wells of a 96-well plate for each of the two samples, and one column was used as a control. After one day, the culture medium was removed, and 100 microliters of extract containing 10% serum was added to each well, while FBS medium was added to the control column. After 24 hours, the extract was removed, and 100 microliters of MTT solution was added to each well. The optical density (OD) of the substance dissolved in isopropanol was calculated at a wavelength of 545 nm using an ELISA reader (StatFax 2000). The well with more cells showed a higher OD than the well with fewer cells, and the relationship below was used to compare the well with more cells with the control sample.

Toxicity (%) 1 – (mean OD of sample/mean OD of control) × 100 **Eq. 5**

Viability (%) = 100 -Toxicity (%) **Eq. 6**

The authors used the change in color concentration of MTT in mitochondria to measure the amount of living cells. The survival percentage of cells was presented in the graphs in the following chapter, indicating the non-toxicity of the samples. For the cell adhesion test, sterilized samples were placed in a sterile 12-well plate, and 20,000 cells in 80 microliters of volume were added to each sample and incubated for 4-5 hours. After cell adhesion, a culture medium containing 10% FBS was added to each well. The samples were fixed with 3.5% gluteraldehyde for 2 hours and then washed with deionized water and varying concentrations of alcohol. Cell adhesion was observed using an AIS2100 SEM. To draw the standard curve for drug release, the authors used cloxacillin at an initial concentration of 2 ppm, which was diluted with PBS to prepare samples with 4 different concentrations. The absorbance of the samples was measured using a UV spectrophotometer at a wavelength of 203 nm, and the area under the peak was calculated for all concentrations. The standard curve of cloxacillin concentration was then plotted based on the amount of UV absorption. The line equation of the standard graph of cloxacillin was obtained as $y = 0.0001x + 0.0001$ with $R^2 = 1$.

To measure the amount of cloxacillin loading and drug release, the authors used UV spectrometry. To prepare the dialysis bag for the release test, it was immersed in a solution containing 2% baking soda by weight and 0.05% EDTA by weight for 30 minutes, washed with double distilled water, and boiled in double distilled water. For the release test, the authors sealed one end of the dialysis bag before adding 4 mg of scaffold containing cloxacillin to it and sealing the other end. The dialysis bag was immersed in 30 ml of PBS solution in a container, which was placed in a water bath at 37°C and shaken. Sampling was conducted every 30 minutes for the first 2 hours, followed by hourly sampling for the next 8 hours. During each sampling interval, 4 ml of PBS solution around the dialysis bag was taken as a sample, and 4 ml of new PBS solution was added to the container. The lid of the container was kept closed during the sampling intervals. The amount of drug released from the scaffold at different time points was calculated using UV spectrometry and expressed as a percentage of drug release according to the cloxacillin release file using the following formula:

Drug release (%) = (concentration of drug loaded in the system / concentration of released drug in different hours) × 100 **Eq. 7**

RESULTS AND DISSCUSION

Various methods, such as electrospinning, rapid prototyping, salt leaching, phase separation, gas foam, spin coating, and melt deposition modeling, have been reported for PCL scaffold fabrication [29-34]. However, the choice of a cost-effective method that uses less time and energy while providing adequate architecture remains challenging. The CS/PCL-HA bilayer scaffold had an average fiber diameter within the range of collagen fibers found in extracellular matrices. The electrospun mats

exhibited no cytotoxic effects in laboratory studies, and HA and KR in the fiber structure synergistically increased cell viability and proliferation. The fibers made by both emulsion and coaxial methods containing HA and KR were found to be efficient for wound healing applications. Fluorescence images showed a significant increase in cell number between days 3 and 7, with no difference observed in cell density for the core and shell structures and the emulsion that did not contain any biogenetic material on the seventh day [38-45]. The optical microscope is a low-cost and non-destructive tool used to study the shape and arrangement of scaffolds. Microscopes with 1000 times magnification are suitable for studying the approximate thickness of the strands produced by 3D printing, which is in the range of micrometers. Figure 4 (a-f) shows the samples were taken to study the effective parameters on the printed scaffold. Figure 4 (a-f) shows the 3D printed scaffold with different angles, while Figure 4 shows the well-coated surface of the scaffolds. SEM images was used for more detailed examination of the morphology. Figure 4 shows the images of printed scaffolds using SEM at 2 different magnifications, illustrating that the 3D printing is done well. Figure 4 is related to the 60 × 60 scaffold, with an average pore size of 0.46 mm in the range of 0.40 to 0.50 mm. The average pore size of the 90 ×45 scaffold in Figure 4 is 0.49 mm, in the range of 0.46 to 0.51 mm. Figure 4 shows the 30 × 30 scaffold with an average pore size of 0.46 mm, in the range of 0.45 to 0.49 mm. Figure 5 (a-c) shows SEM images of uncoated scaffolds fabricated at different angle configurations. Figure 5 (a) shows the scaffold with a 60-60 orientation, Figure 5 (b) illustrates the 45-90 configuration, and Figure 5 (c) shows the 30-30 arrangement. The SEM images show detailed insights into the surface morphology and structural features of the scaffolds, which are critical for evaluating their potential in tissue engineering applications, particularly in relation to cell adhesion and proliferation. Figure 6 (a-c) shows the well-coated surface of all three scaffolds with HA material containing ZnO. EDS analysis was used to determine the amount of elements in the constructed scaffolds. Spectra obtained from the elements in the scaffolds coated with HA and ZnO, along with the drug, are shown in Figure 7 (a-d).

Figure 7 (a-d) shows the chemical formula of HA, zinc oxide, and cloxacillin. Oxygen (O), hydrogen (H), and nitrogen (N) are found in all bio-materials, while chlorine (Cl) is related to medicine. The distribution of elements on the coated scaffolds using Map analysis is illustrated in Figure 8 (a-d), which shows that the Zn element is uniformly placed on the entire surface. Figure 8 (a-d) illustrates the mapping of elemental distribution in covered scaffolds using energy-dispersive EDX. Figure 8 (a) represents the 60-60 scaffold configuration, Figure 8 (b) shows the 45-90 configuration, and Figure 8 (c) shows the 30-30 arrangement. The elemental maps show the spatial distribution of key components within the scaffolds, showing valuable information on the chemical composition and uniformity of the coatings. This analysis is essential for understanding the scaffolds' interactions in tissue engineering applications.

a

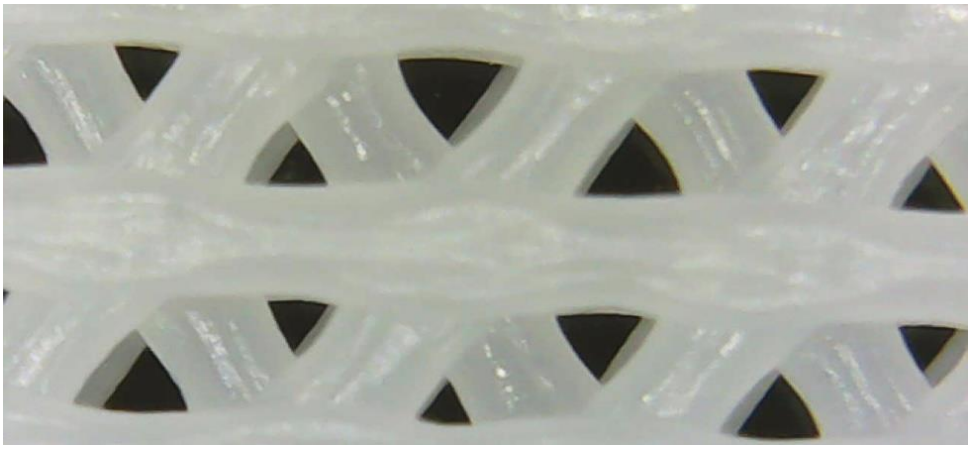

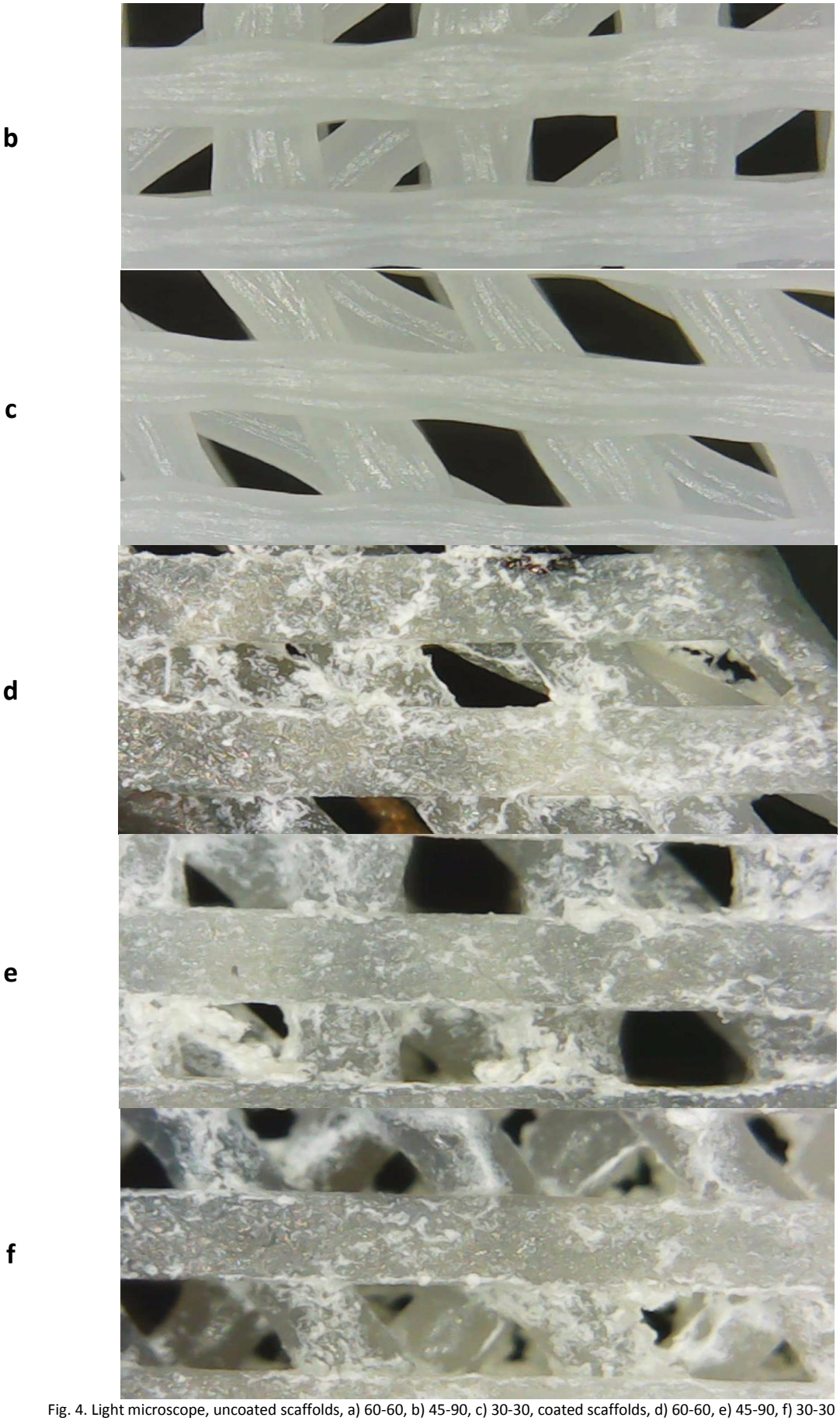

Fig. 4. Light microscope, uncoated scaffolds, a) 60-60, b) 45-90, c) 30-30, coated scaffolds, d) 60-60, e) 45-90, f) 30-30

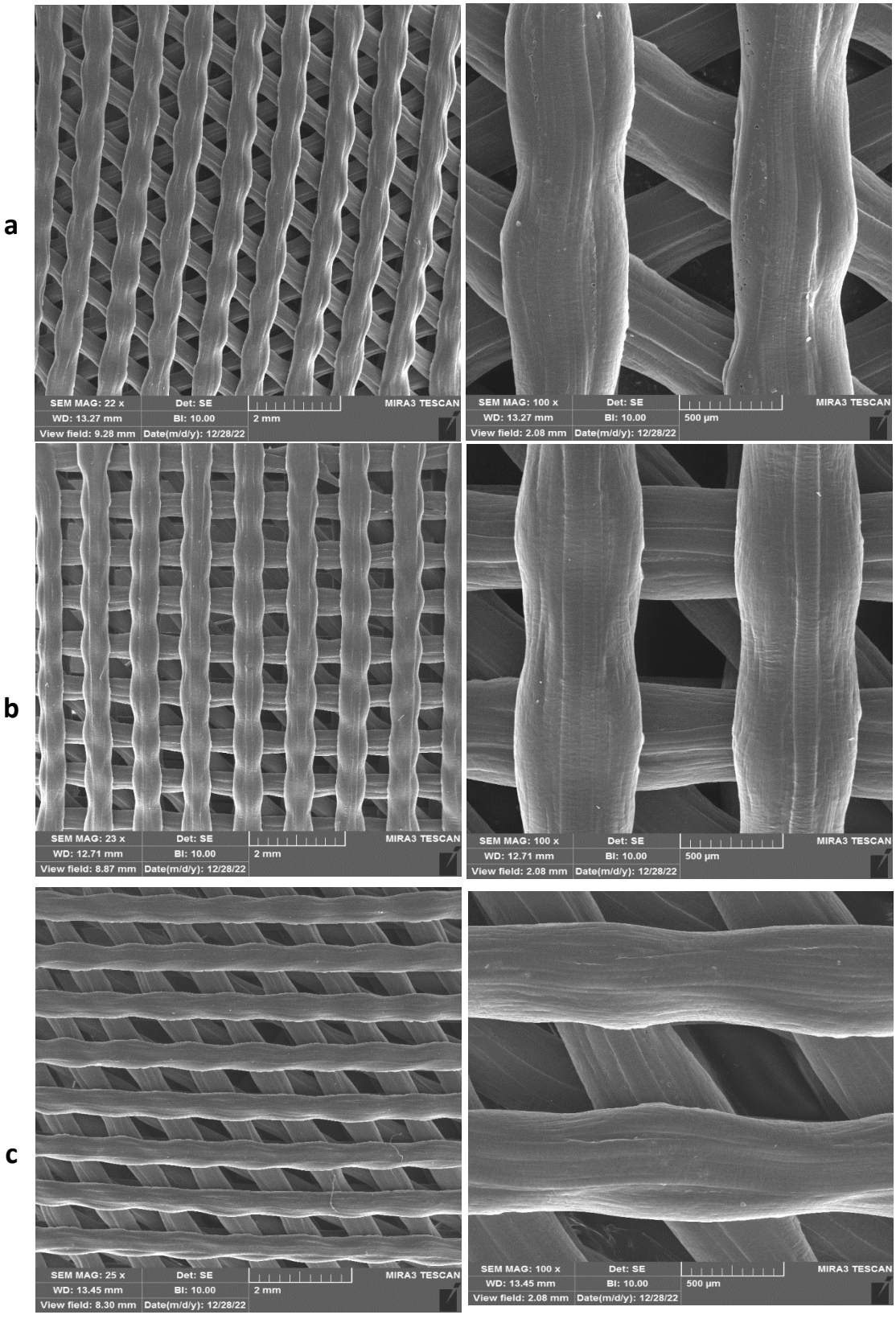

Fig. 5. SEM images of uncoated scaffolds, a) 60-60, b) 45-90, c) 30-30

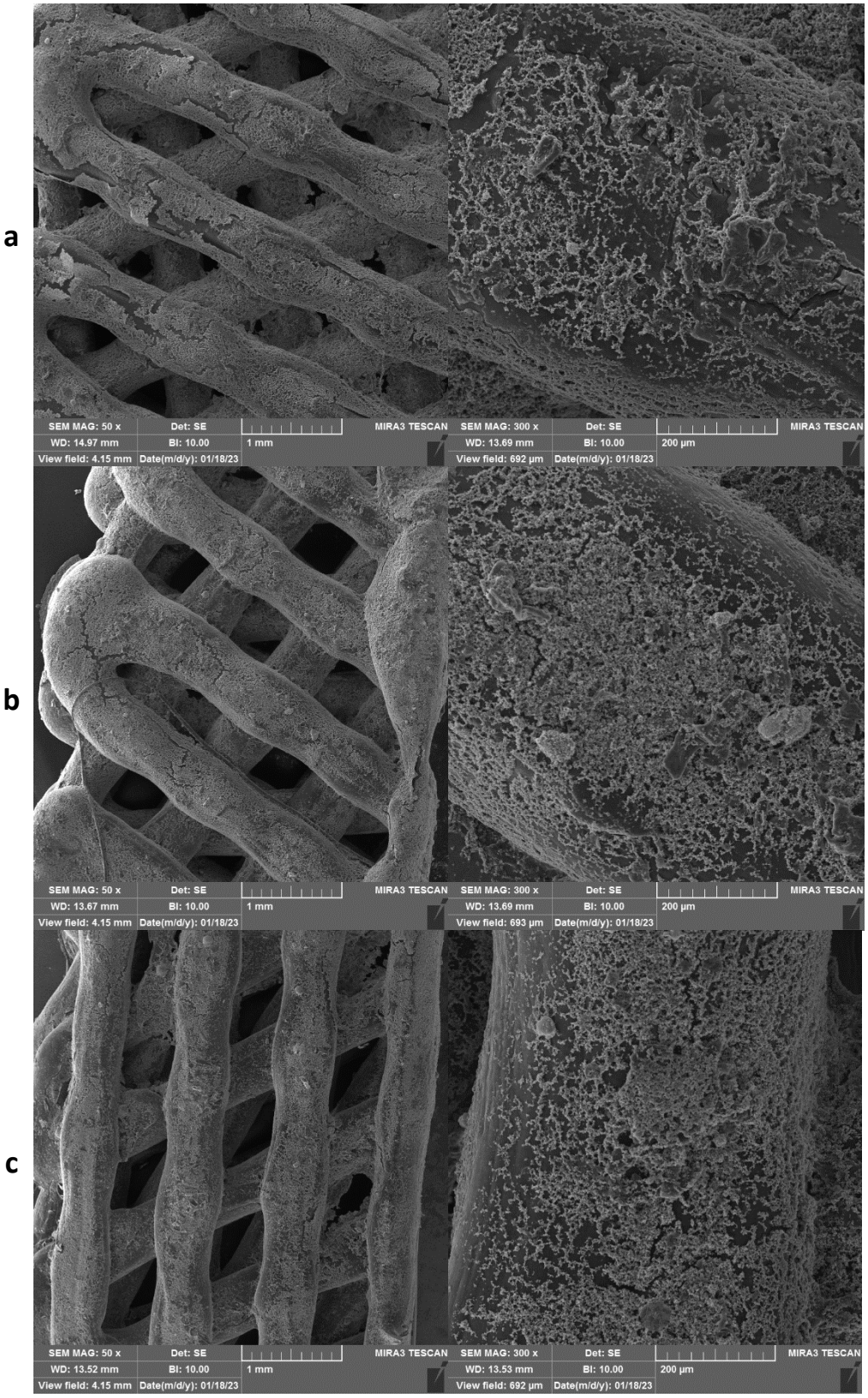

Fig. 6. Scanning electron microscope (SEM), coated scaffolds, a) 60-60, b) 45-90, c) -30

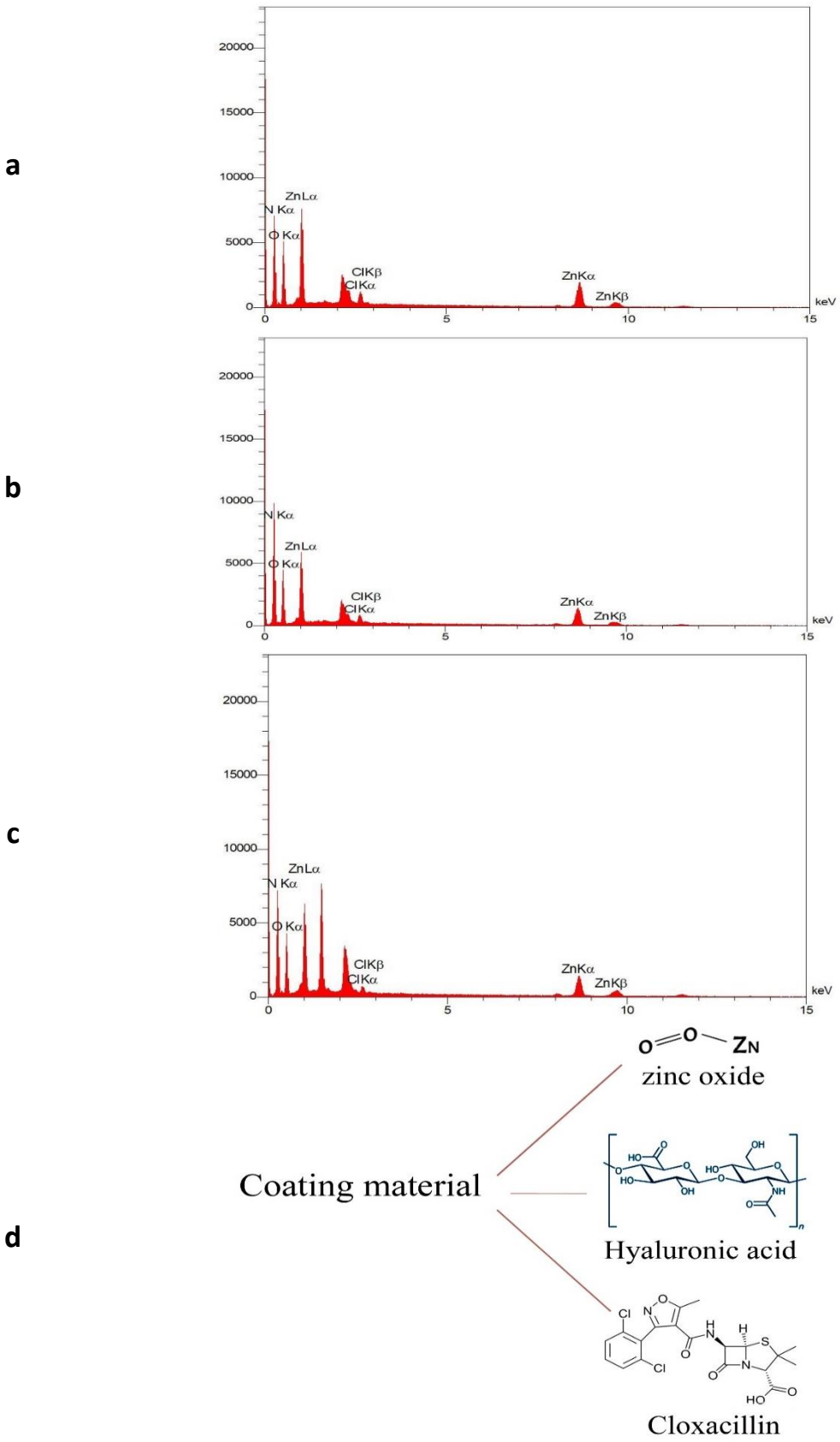

Fig. 7. EDS spectroscopy of coated scaffolds, a) 60-60, b) 45-90, c) 30-30, and d) coated material formula

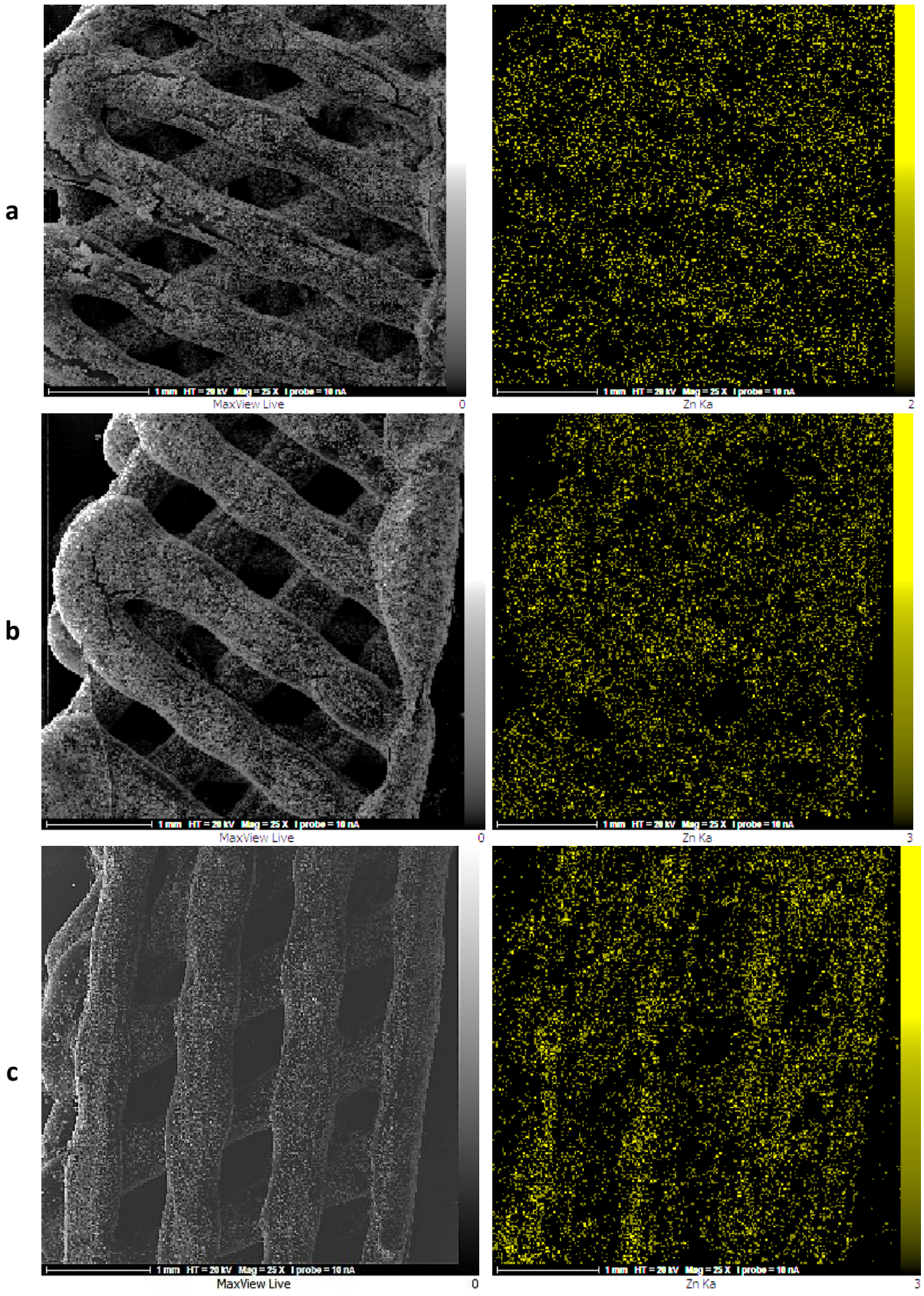

Fig. 8. Pointing of elements using Map from covered scaffolds, a) 60-60, b) 45-90, and c) 30-30

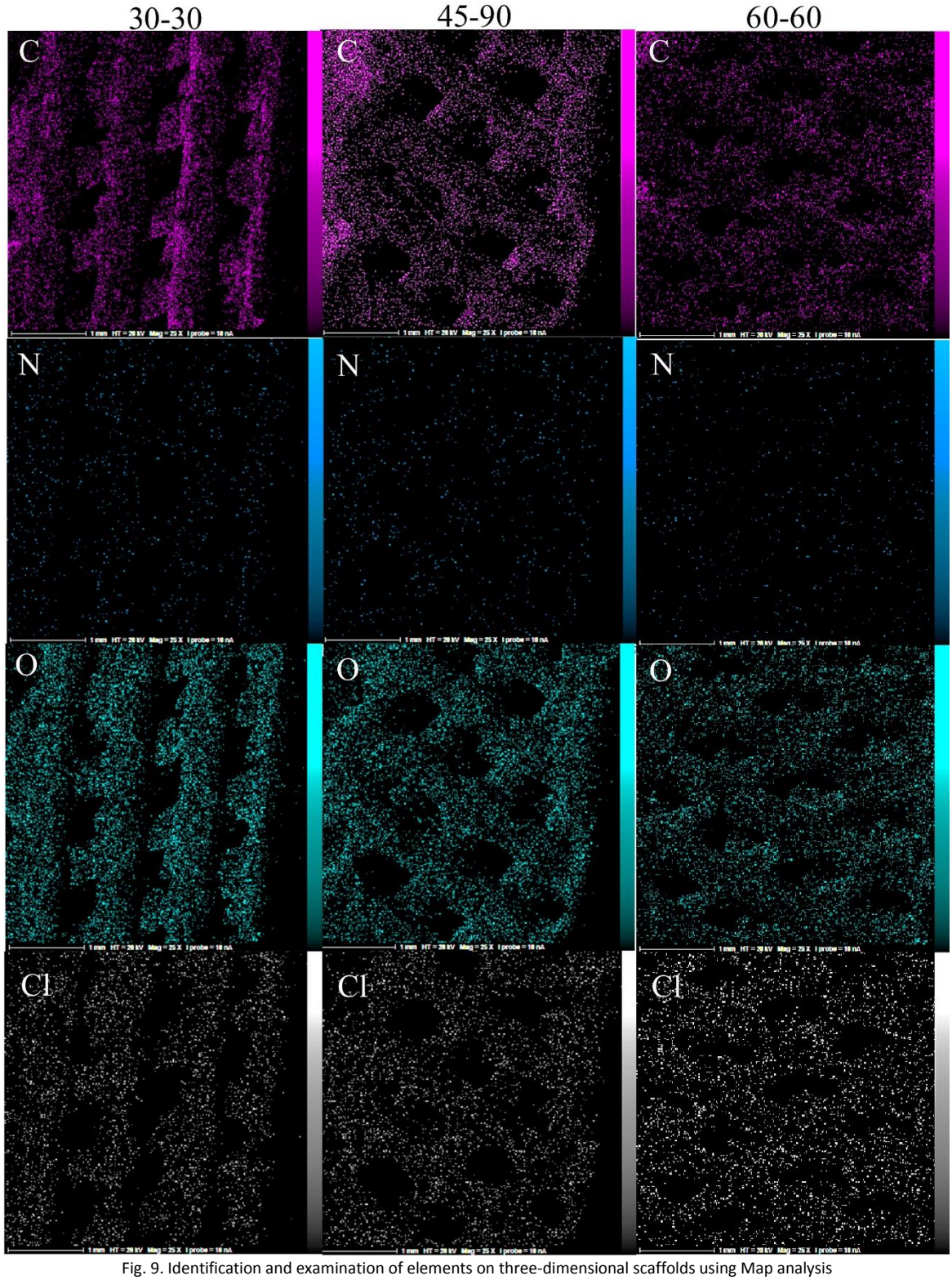

Fig. 9. Identification and examination of elements on three-dimensional scaffolds using Map analysis

Table 5. Examination of mechanical properties of scaffolds using tensile test

sample	%E	Young's Modulus (MPa)
30-30	17.87%	1.32
60-60	15.46%	0.73
90-45	13.68%	0.45

Figure 9 shows the elements on each scaffold, indicating that the placement of elements is uniform due to the well-coated surface of the scaffolds. To evaluate the mechanical properties of uncoated scaffolds, a tensile test was conducted, and Table 5 shows the amount of stretch, stretch percentage, and elastic modulus. The elastic modulus for the 30-30 scaffold is higher than that of the other scaffolds (1.32 MPa), while the Young's modulus for the 60-60 and 45-90 scaffolds is 0.73 and 0.45 MPa, respectively. Many studies show that decreasing the angles of the strands improves mechanical properties. The design of the strands for all three scaffolds is the same in size but with different angles, as shown in Figure 10 (a-d). Decreasing the angles results in smaller pores and increased mechanical properties, as illustrated in Figure 10 (a-d). The force-tension diagram is shown in Figure 10. The moist healing environment is favorable for the growth of granulation, facilitates cell proliferation, and promotes wound healing according to previous research [46-52]. The swelling properties of scaffolds immersed in distilled water and phosphate buffered salt at various times were investigated. Figure 11 shows the percentage of inflation of scaffolds with and without coating, indicating that the percentage of inflation can be divided into two categories. The lower diagrams in the figure, which are related to scaffolds without coating, show a small difference in their swelling rate of 25-28% after 120 minutes, as the material used (PCL) is the same for all scaffolds. The upper diagrams in the figure, which are related to coated scaffolds with different angles, show a higher inflation rate of 42-47%.The swelling and deformation of porous media under varying saturation conditions is a common phenomenon in geotechnical, engineering, and biological tissue issues. Numerical models have been developed to study swelling and deformation of materials, such as the model for inflation based on the exploitation of the entropy inequality, and a numerical model. These models explain the effect of swelling and deformation on hydraulic parameters like the capillary pressure-saturation curve, permeability, and porosity using empirical equations. The presence of pore water inside a porous medium affects its behavior during deformation, which in turn affects its hydraulic properties. Any change in the structure of the porous medium causes a change in its permeability, such as a decrease in porosity resulting in a decrease in permeability. The presence of pores in the 3D scaffolds is an effective reason for water absorption according to the researchers' studies.

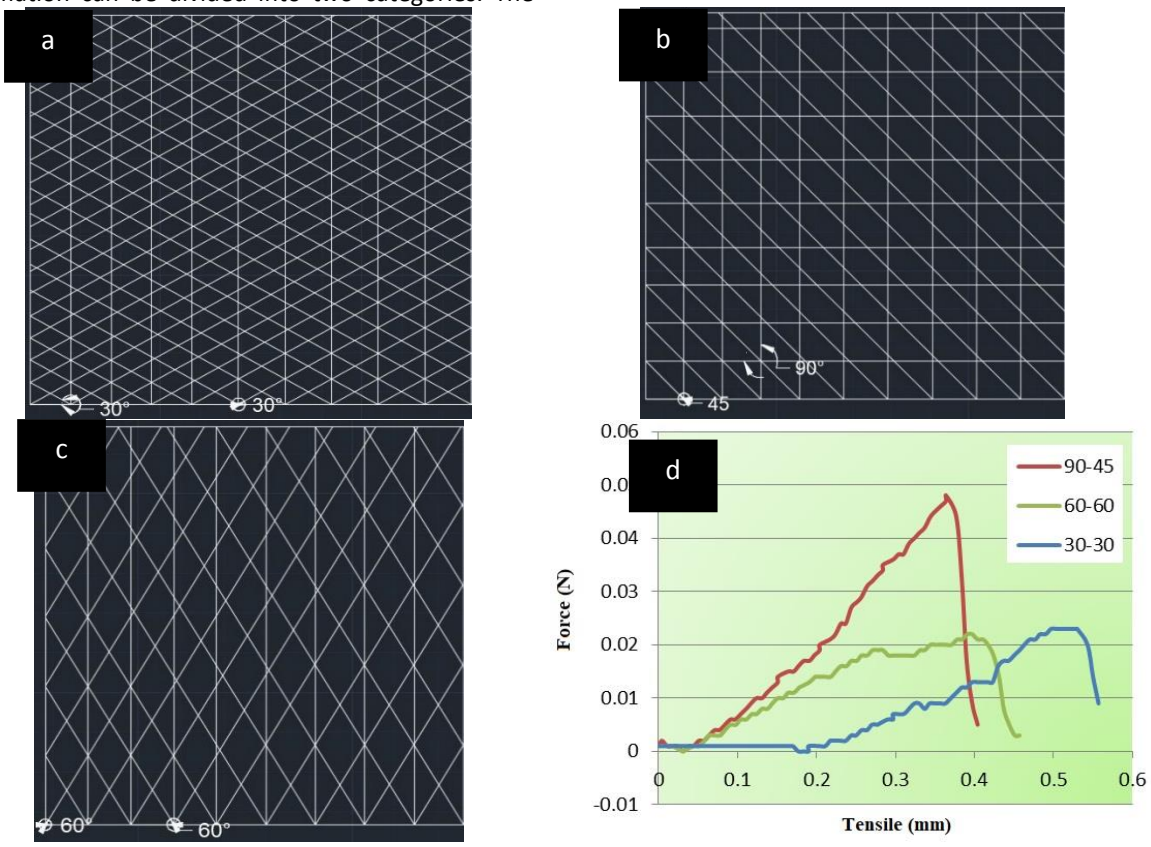

Fig. 10. Design of three-dimensional scaffolds and placement of strands, a) 90-45, b) 30-30, c) 60-60, d) diagram of mechanical properties of scaffolds based on force-tension

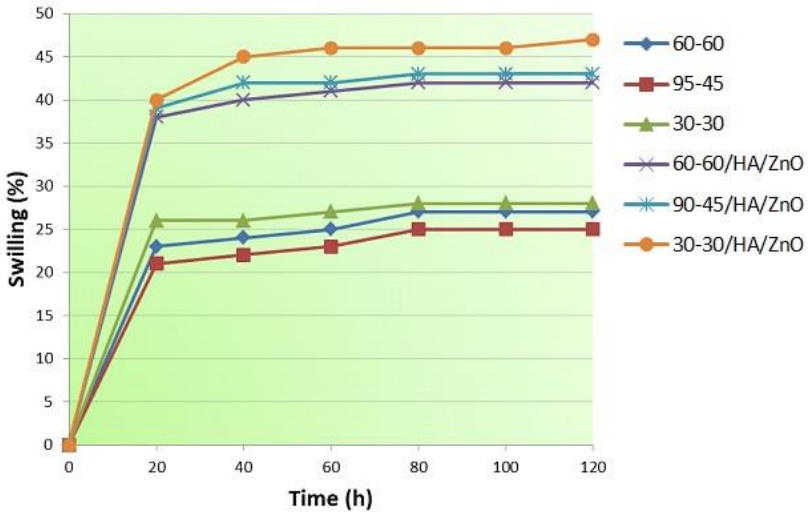

Fig. 11. Checking the swelling percentage of the scaffold with and without coating using HA and ZnO for 120 minutes.

The results obtained indicate that the addition of HA increases swelling, which is consistent with similar findings in other studies. This is because HA can loosen the structure of the hydrogel membrane and allow molecular chains to expand more easily. Scaffolds made of HA and ZnO show good swelling behavior due to the hydrophilic nature of the HA molecule, which is a common hydrophilic polymer. The coated scaffolds maintain stable swelling ability due to the stronger intermolecular hydrogen bonds between the hyaluronic acid/ZnO layer and PCL. The high water absorption of scaffolds is attributed to the hydrophilic groups in the HA molecular chains and the porosity of the 3D scaffold, which facilitates water absorption. The ability of all coated scaffolds to swell makes them suitable for stable scaffolds in tissue engineering applications, preventing the loss of body fluids and nutrients in *in vivo* experiments, and increasing cell attachment and proliferation on the 3D scaffold. Therefore, they can be ideal scaffolds for tissue engineering therapy .Table 3 shows the percentage of degradation of 3D scaffolds with and without coating when placed in phosphate buffer salt for 20 days. Scaffolds without coating show a degradation rate of 14-16% in 20 days, which increases with the addition of a coating to a range of 24-26%. Figure 12 shows the degradation process on different days, illustrating that the coated scaffolds undergo slow degradation on the 20th day, which is not significantly different from the 15th day. This is because the HA is completely destroyed and separated from the surface of the scaffold, while the degradation of PCL occurs slowly.

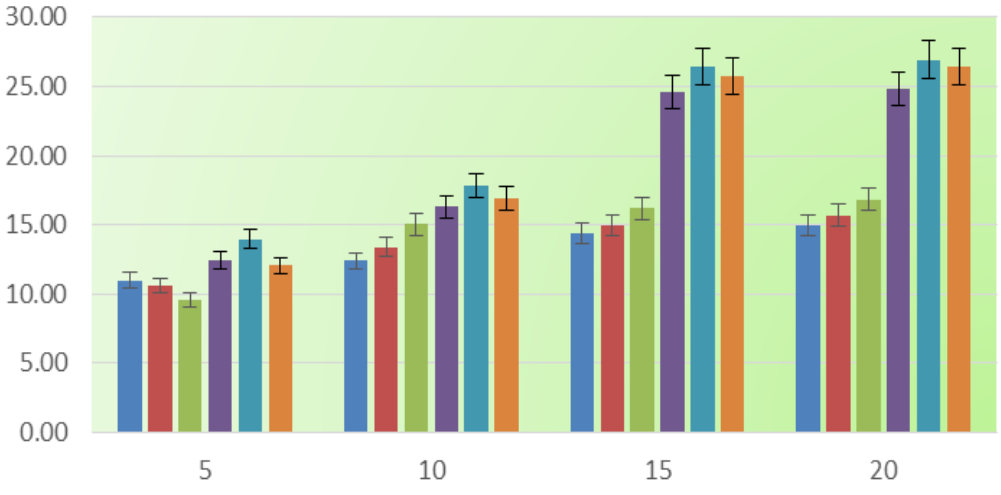

Fig. 12. Investigation of the percentage of biodegradability of the scaffold with and without coating using HA and ZnO for 20 days

In the absence of HA coating and ZnO, the 3D-scaffold showed less degradation. The presence of poly-caprolactone in the scaffold slows down the degradation process, making it a potential option for use in biological scaffolds due to its biodegradability, non-toxicity, and biocompatibility with many drugs and biopolymers. Moreover, the slower degradation rate of poly-caprolactone compared to other biodegradable polymers makes it suitable for constructing tissue engineering scaffolds that require longer degradation times. Ali et al. [18] investigated the degradation of poly-caprolactone in implantable implants using GPC, DSC, and SEM tests and hypothesized that HO radical is an important reason for the degradation of poly-caprolactone. Chen et al. [19] compared the in vitro degradation behavior of poly-caprolactone microparticles and poly-caprolactone film in PBS solution with pH 7.4 at 37 ± 1°C and found that the form of poly-caprolactone has no significant effect on its degradation rate, indicating homogeneous degradation. Huang et al. [20] found that the degradation rate of poly-caprolactone is affected by the percentage of other substances present. They created a film of poly-caprolactone and polyvinyl alcohol, which showed cracks after dissolving in water due to the dissolution of polyvinyl alcohol and subsequent degradation of poly-caprolactone. Hydrolysis is a major mechanism of degradation in the presence of tissue water, and research on hydrolytic degradation of tissue engineering scaffolds with biodegradable polymers is essential for biodegradation. Over time, structures in a water-based degradation environment undergo chemical interactions and bond failure, with all polymer hydrogel scaffolds primarily subjected to bulk and surface degradation facilitated by hydrolysis [46-51]. These changes lead to weight reduction of the hydrogel scaffolds, which absorb physiological solution and swell during the degradation period. Hydrolysis is facilitated by the diffusion of water inside the matrix, ultimately leading to significant destruction of the scaffolds.

Recent research has demonstrated significant advancements in biomaterials for tissue engineering, particularly through the integration of various polymers and composites. One study developed a porous sodium alginate-$CaSiO_3$ polymer reinforced with graphene nanosheets, highlighting the importance of optimal fabrication techniques [46-53]. Many other investigation explored the synergistic effects of magnetic nanoparticles for hyperthermia therapy and controlled drug delivery, showcasing innovative approaches for bone substitutes [54-58]. Additionally, research into self-healing polymers suggests potential enhancements in scaffold longevity [59-62]. Efforts have also been made to improve osseointegration and mechanical properties in orthopedic applications using diverse composite materials. Many research results show the need for continued exploration of scaffold design, mechanical stimuli, and drug delivery systems to optimize biocompatibility and functionality in biomedical applications, paving the way for future innovations in regenerative medicine [62-67]. Cloxacillin is frequently used to treat infections caused by penicillinase-producing staphylococcal species. This study evaluated the release rate of cloxacillin from the 60-60/HA/ZnO scaffold. The drug release occurred in two stages with different gradients, with an initial explosive release of approximately 16% of the loaded drug due to surface abrasion and release of drugs attached to the surface of the scaffold, followed by a slower release due to penetration inside the scaffold and continued degradation of the polymer, resulting in a total release rate of 27%. The MTT test confirmed the non-toxicity of the prepared system and investigated the effect of cloxacillin release on the proliferation and survival of fibroblast cells. Biocompatibility was examined for scaffolds with and without coating, with the coated scaffold showing better biocompatibility due to the presence of HA, an important glycosaminoglycan of the ECM.

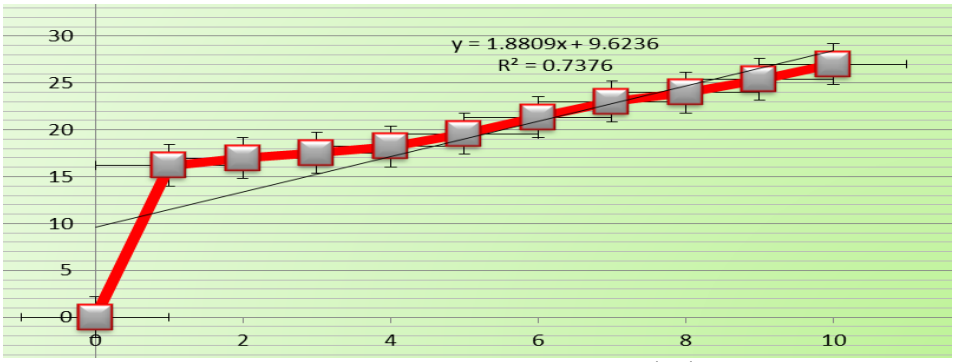

Fig. 13. Release percentage of cloxacillin drug from 60-60/HA/ZnO scaffold

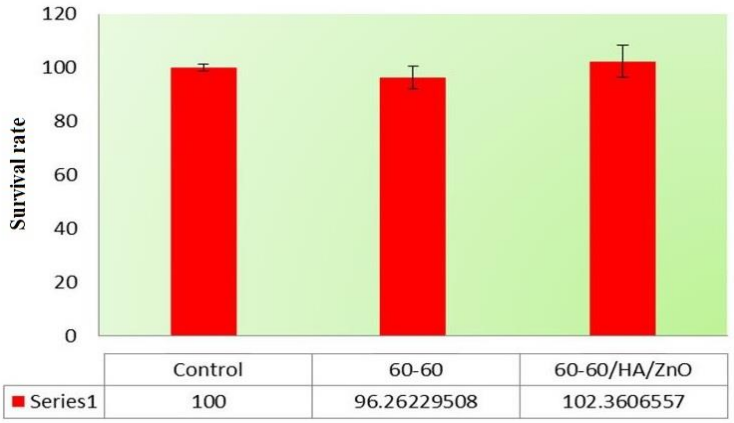

Fig. 14. Examining the biocompatibility of scaffolds with and without coating using the MTT method

Figure 13 illustrates the release percentage of cloxacillin from the 60-60/HA/ZnO scaffold over a specified time period. Cloxacillin, an antibiotic effective against certain bacterial infections, was incorporated into the scaffold matrix to evaluate its release profile. The data presented reflect the cumulative drug release at various time intervals, showcasing how the scaffold facilitates the controlled release of the drug. This analysis is crucial for understanding the scaffold's potential for sustained therapeutic effects in tissue engineering applications. The incorporation of HA and ZnO is expected to influence the release kinetics, with HA enhancing biocompatibility and ZnO providing antibacterial properties. The results show the scaffold's ability to deliver cloxacillin effectively, suggesting its potential utility in preventing infections at the implantation site while promoting tissue regeneration. Figure 14 shows the results of a biocompatibility assessment conducted on scaffolds both with and without coating, utilizing the MTT assay. The MTT method is a widely recognized colorimetric assay that measures cell viability based on the metabolic activity of living cells. In this analysis, scaffolds were exposed to cultured cells, and the subsequent conversion of MTT to formazan crystals was quantified, providing insights into the scaffolds' compatibility with biological tissues. The comparison between coated and uncoated scaffolds highlights differences in cell viability, offering critical implications for their potential applications in tissue engineering. Enhanced cell proliferation on coated scaffolds suggests improved biocompatibility, which is essential for successful integration and functionality *in vivo*. Recent studies have highlighted the significant role of salivary C-reactive protein (CRP) in both systemic and oral disorders, indicating its potential as a diagnostic marker. Research has also examined periodontal health and hygiene practices among diabetic and nondiabetic adolescents, revealing important differences that could inform preventive strategies [65-70]. Additionally, the relationship between clinical findings and oral health in rheumatoid arthritis patients underscores the interconnectedness of systemic conditions and oral status. These insights contribute to a better understanding of how systemic diseases impact oral health and vice versa. Fibroblast cells, which continuously regenerate the connective tissue by synthesizing the ECM and secreting growth factors, were used for the biocompatibility study. The uncoated scaffold exhibited 96% biocompatibility, while the coated scaffold exhibited 102% biocompatibility. While the current study has demonstrated the potential of PCL/ HA scaffolds for tissue engineering applications, several limitations should be addressed in future research. Firstly, the study was conducted *in vitro*, and the performance of the scaffolds under *in vivo* conditions needs evaluation to better understand their suitability for real-world clinical applications; factors such as the host immune response, vascularization, and long-term integration with surrounding tissues should be investigated to ensure the scaffolds' viability and efficacy in a physiological environment. Additionally, drug release kinetics could be further optimized by exploring different coating compositions and techniques to achieve a more controlled and sustained release profile, while investigating various drug loadings and their influence on the scaffold's mechanical and biological properties would also be valuable. Furthermore, expanding the study to include a wider range of cell types, such as osteoblasts or chondrocytes, could provide insights into the scaffolds' suitability for different tissue engineering applications. Future research should also focus on scaling up the manufacturing process and

evaluating the feasibility of mass production to facilitate the clinical translation of these scaffolds. Addressing these limitations and exploring these avenues for further research will help advance the development of these biomimetic scaffolds and their potential for tissue regeneration.

CONCLUSION

Tissue engineering and the repair of damaged tissues are critical areas in medical science. The production of scaffolds made of natural and synthetic polymers with favorable properties for the purpose of reconstructing damaged tissues has been expanding. These scaffolds may be made from natural, artificial, or mineral materials, which must be biocompatible and biodegradable. Hydrophilicity is also an important property for effective scaffolds, as a hydrophilic surface promotes enhanced cell adhesion and growth. However, most synthetic polymers lack the necessary hydrophilicity for use in tissue engineering. This study utilized 3D printing techniques to create a three-dimensional scaffold based on poly-caprolactone, with different angles of placement. The scaffolds were then coated in a solution containing HA, ZnO, and drugs. Morphological examination was done using an optical microscope and a SEM, with element identification analysis conducted using elemental spectroscopy and mapping. The swelling and biodegradability of the scaffolds were measured in phosphate buffered salt solution, and the mechanical and biological properties were determined using tensile tests, bioavailability and cell viability. A drug release test was also conducted using a dialysis bag. The results showed that the coated scaffolds had better swell and biodegradability, and a higher rate of drug release than the uncoated scaffolds. The coated scaffolds also exhibited better biocompatibility. Thus, the study supports the potential of using poly-caprolactone-based scaffolds in tissue engineering. The study highlights the potential of poly-caprolactone/ HA scaffolds for tissue engineering but identifies several limitations for future research. Key areas include evaluating scaffold performance in vivo, investigating host immune responses, vascularization, and long-term integration. Optimizing drug release kinetics through different coating techniques and exploring various drug loadings are crucial. Additionally, including more cell types, such as osteoblasts or chondrocytes, and focusing on scaling up manufacturing for clinical translation may advance the development of these scaffolds for tissue regeneration.

AVAILABILITY OF DATA AND MATERIALS

The datasets supporting the conclusions of this study are included within the article.

CONFLICTS OF INTEREST

The authors have declared that no competing interests exist.

ACKNOWLEDGEMENT

This work was supported by the scientific and technological innovation project.

REFERENCES

1. Wang Q, Yan J, Yang J, Li B. Nanomaterials promise better bone repair. Mater Today. 2016; 19(8):451-463.
2. Basirun WJ, Nasiri-Tabrizi B, Baradaran S. Overview of hydroxyapatite–graphene nanoplatelets composite as bone graft substitute: mechanical behavior and in-vitro biofunctionality. Critical reviews in solid state and materials sciences. 2018; 43(3):177-212.
3. Alves Cardoso D, Jansen JA, G. Leeuwenburgh SC. Synthesis and application of nanostructured calcium phosphate ceramics for bone regeneration. Journal of Biomedical Materials Research Part B: Applied Biomaterials. 2012; 100(8):2316-2326.
4. Oryan A, Alidadi S, Moshiri A, Maffulli N. Bone regenerative medicine: classic options, novel strategies, and future directions. J Orthop Surg Res. 2014; 9:1-27.
5. Wang N, Dheen ST, Fuh JY, Kumar AS. A review of multi-functional ceramic nanoparticles in 3D printed bone tissue engineering. Bioprinting. 2021; 23:e00146.
6. Xue X, Hu Y, Wang S, Chen X, Jiang Y, Su J. Fabrication of physical and chemical crosslinked hydrogels for bone tissue engineering. Bioact Mater. 2022; 12:327-39.
7. Shalumon KT, Anulekha KH, Chennazhi KP, Tamura H, Nair SV, Jayakumar R. Fabrication of chitosan/poly (caprolactone) nanofibrous scaffold for bone and skin tissue engineering. Int J Biol Macromol. 2011; 48(4):571-576.
8. El-Aassar MR, Ibrahim OM, Fouda MM, El-Beheri NG, Agwa MM. Wound healing of nanofiber comprising Polygalacturonic/Hyaluronic acid embedded silver nanoparticles: In-vitro and in-vivo studies. Carbohydr Polym. 2020; 238:116175.
9. Nabipour I. The future of 3D printing technology in biomedicine. Iran South Med J. 2015;18(3):680-689.
10. Hwang HJ, Chung WH, Kim HS. In situ monitoring of flash-light sintering of copper nanoparticle ink for printed electronics. Nanotechnology. 2012;23(48):485205.
11. S. Shah S, Lee JY, Verkhoturov S, Tuleuova N, Schweikert EA, Ramanculov E, Revzin A. Exercising spatiotemporal control of cell attachment with optically transparent microelectrodes. Langmuir. 2008; 24(13):6837-6844.

12. Nikolovski J, Mooney DJ. Smooth muscle cell adhesion to tissue engineering scaffolds. Biomaterials. 2000;21(20):2025-2032.
13. Liu Y, Li T, Han Y, Li F, Liu Y. Recent development of electrospun wound dressing. Curr Opin Biomed Eng. 2021;17:100247.
14. Sionkowska A, Gadomska M, Musiał K, Piątek J. Hyaluronic acid as a component of natural polymer blends for biomedical applications: a review. Molecules. 2020;25(18):4035.
15. Ghomi H, Sepyani A. Fabrication and evaluation of (chitosan/poly-vinyl-pyrrolidone) scaffold properties containing gum tragacanth by freeze-drying method. Adv Process Eng Mater. 2020; 14(1):27-43.
16. Vieira AC, Vieira JC, Ferra JM, Magalhães FD, Guedes RM, Marques AT. Mechanical study of PLA–PCL fibers during in vitro degradation. J Mech Behav Biomed Mater. 2011;4(3):451-460.
17. Sun H, Mei L, Song C, Cui X, Wang P. The in vivo degradation, absorption and excretion of PCL-based implant. Biomaterials. 2006;27(9):1735-1740.
18. Ali SA, Zhong SP, Doherty PJ, Williams DF. Mechanisms of polymer degradation in implantable devices: I. Poly (caprolactone). Biomaterials. 1993;14(9):648-656.
19. Chen DR, Bei JZ, Wang SG. Polycaprolactone microparticles and their biodegradation. Polym Degrad Stab. 2000;67(3):455-459.
20. Huang D, Hu ZD, Ding Y, Zhen ZC, Lu B, Ji JH, Wang GX. Seawater degradable PVA/PCL blends with water-soluble polyvinyl alcohol as degradation accelerator. Polym Degrad Stab. 2019;163:195-205.
21. Basu P, Saha N, Alexandrova R, Saha P. Calcium phosphate incorporated bacterial cellulose-polyvinylpyrrolidone based hydrogel scaffold: structural property and cell viability study for bone regeneration application. Polymers. 2019;11(11):1821.
22. Hashemi SS, Rajabi S, Mahmoudi R, Ghanbari A, Jafari Barmak M. The Investigation of Proliferation of Fibroblasts on Chitosan Scaffold in the Presence of Hyaluronic Acid. Armaghane Danesh. 2018;23(2):134-145.
23. Liang H, Mirinejad MS, Asefnejad A, Baharifar H, Li X, Saber-Samandari S, Toghraie D, Khandan A. Fabrication of tragacanthin gum-carboxymethyl chitosan bio-nanocomposite wound dressing with silver-titanium nanoparticles using freeze-drying method. Mater Chem Phys. 2022; 279:125770.
24. Karimi M, Asefnejad A, Aflaki D, Surendar A, Baharifar H, Saber-Samandari S, Khandan A, Khan A, Toghraie D. Fabrication of shapeless scaffolds reinforced with baghdadite-magnetite nanoparticles using a 3D printer and freeze-drying technique. J Mater Res Technol. 2021;14:3070-3079.
25. Salmani MM, Hashemian M, Khandan A. Therapeutic effect of magnetic nanoparticles on calcium silicate bioceramic in alternating field for biomedical application. Ceram Int. 2020;46(17):27299-27307.
26. Raisi A, Asefnejad A, Shahali M, Doozandeh Z, Kamyab Moghadas B, Saber-Samandari S, Khandan A. A soft tissue fabricated using a freeze-drying technique with carboxymethyl chitosan and nanoparticles for promoting effects on wound healing. J Nanoanalysis. 2020;7(4):262-274.
27. Jamnezhad S, Asefnejad A, Motififard M, Yazdekhasti H, Kolooshani A, Saber-Samandari S, Khandan A. Development and investigation of novel alginate-hyaluronic acid bone fillers using freeze drying technique for orthopedic field. Nanomed Res J. 2020;5(4): 306-315.
28. Iranmanesh P, Ehsani A, Khademi A, Asefnejad A, Shahriari S, Soleimani M, Ghadiri Nejad M, Saber-Samandari S, Khandan A. Application of 3D bioprinters for dental pulp regeneration and tissue engineering (porous architecture). Transp Porous Media. 2022; 142(1):265-293.
29. Attaeyan A, Shahgholi M, Khandan A. Fabrication and characterization of novel 3D porous Titanium-6Al-4V scaffold for orthopedic application using selective laser melting technique. Iran J Chem Chem Eng. 2024;43(1).
30. Moarrefzadeh A, Morovvati MR, Angili SN, Smaisim GF, Khandan A, Toghraie D. Fabrication and finite element simulation of 3D printed poly L-lactic acid scaffolds coated with alginate/carbon nanotubes for bone engineering applications. Int J Biol Macromol. 2023; 224:1496-1508.
31. Safaei MM, Abedinzadeh R, Khandan A, Barbaz-Isfahani R, Toghraie D. Synergistic effect of graphene nanosheets and copper oxide nanoparticles on mechanical and thermal properties of composites: Experimental and simulation investigations. Mater Sci Eng B. 2023; 289:116248.
32. Angili SN, Morovvati MR, Kardan-Halvaei M, Saber-Samandari S, Razmjooee K, Abed AM, Toghraie D, Khandan A. Fabrication and finite element simulation of antibacterial 3D printed Poly L-lactic acid scaffolds coated with alginate/magnesium oxide for bone tissue regeneration. Int J Biol Macromol. 2023;224:1152-1165.
33. Fatalla AA, Arzani S, Veseli E, Khademi A, Khandan A, Fahmy MD, Mirmohammadi H, Hasselgren G, Bang H, Kolahi J, Kelishadi R. Revolutionizing systematic reviews and meta-analyses: the role of artificial intelligence in evidence synthesis. Dent Hypotheses. 2023;14(4):93-94.
34. Mirmohammadi H, Kolahi J, Khandan A. Bibliometric analysis of dental preprints which published in 2022. Dent Hypotheses. 2023;14(1):1-2.
35. Sotoudeh A, Darbemamieh G, Goodarzi V, Shojaei S, Asefnejad A. Tissue engineering needs new biomaterials: Poly (xylitol-dodecanedioic acid)–co-polylactic acid (PXDDA-co-PLA) and its nanocomposites. Eur Polym J. 2021;152:110469.
36. Mirzadeh S, Asefnejad A, Khonakdar HA, Jafari SH. Improved surface properties in spray-coated PU/TiO2/graphene hybrid nanocomposites through nonsolvent-induced phase separation. Surf Coat Technol. 2021;405:126507.
37. Biazar E, Beitollahi A, Rezayat SM, Forati T, Asefnejad A, Rahimi M, Zeinali R, Ardeshir M, Hatamjafari F, Sahebalzamani A, Heidari M. Effect of the mechanical activation on size reduction of crystalline

acetaminophen drug particles. Int J Nanomedicine. 2009:283-287.
38. Ghafari Y, Asefnejad A, Ogbemudia DO. Gold nanoparticles in biomedicine: advancements in cancer therapy, drug delivery, diagnostics, and tissue regeneration. Sci Hypotheses. 2024; 1:21-35.
39. Sheikhbahei E, Ari AA. Harnessing the power of emerging digital technologies for improved sustainability and productivity in biomedical engineering and neuroscience. Sci Hypotheses. 2024;1:47-52.
40. Moghadas BK, Ghanbari N, Nasri P. Advancements in Nanoparticle Biosensors: Applications, Properties, and Considerations for Improving Performance and Detection Capabilities. Sci Hypotheses. 2024;1:53-71.
41. Shirani K, Sheikhbahaei E, Torkpour Z, Nejad MG, Moghadas BK, Ghasemi M, Aghdam HA, Ehsani A, Saber-Samandari S, Khandan A. A narrative review of COVID-19: the new pandemic disease. Iran J Med Sci. 2020;45(4):233.
42. Kordjamshidi A, Saber-Samandari S, Nejad MG, Khandan A. Preparation of novel porous calcium silicate scaffold loaded by celecoxib drug using freeze drying technique: Fabrication, characterization and simulation. Ceram Int. 2019;45(11):14126-14135.
43. Iranmanesh P, Ehsani A, Khademi A, Asefnejad A, Shahriari S, Soleimani M, Ghadiri Nejad M, Saber-Samandari S, Khandan A. Application of 3D bioprinters for dental pulp regeneration and tissue engineering (porous architecture). Transp Porous Media. 2022;142(1):265-293.
44. Khandan A, Ozada N, Saber-Samandari S, Nejad MG. On the mechanical and biological properties of bredigite-magnetite (Ca7MgSi4O16-Fe3O4) nanocomposite scaffolds. Ceram Int. 2018;44(3): 3141-3148.
45. Ghayour H, Abdellahi M, Nejad MG, Khandan A, Saber-Samandari S. Study of the effect of the Zn 2+ content on the anisotropy and specific absorption rate of the cobalt ferrite: the application of Co 1− x Zn x Fe 2 O 4 ferrite for magnetic hyperthermia. J Australas Ceram Soc. 2018;54: 223-230.
46. Foroutan S, Hashemian M, Khosravi M, Nejad MG, Asefnejad A, Saber-Samandari S, Khandan A. A porous sodium alginate-CaSiO 3 polymer reinforced with graphene nanosheet: fabrication and optimality analysis. Fibers Polym. 2021;22: 540-549.
47. Salmani MM, Hashemian M, Yekta HJ, Nejad MG, Saber-Samandari S, Khandan A. Synergic effects of magnetic nanoparticles on hyperthermia-based therapy and controlled drug delivery for bone substitute application. J Supercond Nov Magn. 2020;33: 2809-2820.
48. Sun C, Yarmohammadi A, Isfahani RB, Nejad MG, Toghraie D, Fard EK, Saber-Samandari S, Khandan A. Self-healing polymers using electrosprayed microcapsules containing oil: Molecular dynamics simulation and experimental studies. J Mol Liq. 2021;325:115182.
49. Bagherifard A, Joneidi Yekta H, Akbari Aghdam H, Motififard M, Sanatizadeh E, Ghadiri Nejad M, Esmaeili S, Saber-Samandari S, Sheikhbahaei E, Khandan A. Improvement in osseointegration of tricalcium phosphate-zircon for orthopedic applications: an in vitro and in vivo evaluation. Med Biol Eng Comput. 2020;58:1681-1693.
50. Hashemi SA, Esmaeili S, Nejad MG, Saber-Samandari S, Sheikhbahaei E, Kordjamshidi A, Khandan A. Micro-Finite Element Model to Investigate the Mechanical Stimuli in Scaffolds Fabricated via Space Holder Technique for Cancellous Bone. Int J Adv Des Manuf Technol. 2020;13(1).
51. Esmaeili S, Shahali M, Kordjamshidi A, Torkpoor Z, Namdari F, Saber-Samandari S, Nejad MG, Khandan A. An artificial blood vessel fabricated by 3D printing for pharmaceutical application. Nanomed J. 2019;6(3):183-194.
52. Khandan A, Karamian E, Bonakdarchian M. Mechanochemical synthesis evaluation of nanocrystalline bone-derived bioceramic powder using for bone tissue engineering. Dent Hypotheses. 2014;5(4):155-161.
53. Khandan, A., Nassireslami, E., Saber-Samandari, S., & Arabi, N. (2020). Fabrication and characterization of porous bioceramic-magnetite biocomposite for maxillofacial fractures application. Dent Hypotheses, 11(3), 74-85.
54. Hasselgren, G. (2023). Collaboration Over Borders: From Clinical Dentistry To Quantum Biology. Dent Hypotheses, 14(2), 43-44.
55. Ngoc VT, Ha PT, Hung DT, Anh NV. Management of clear aligner-related severe enamel demineralization with A modified resin infiltration technique: a case report. Dent Hypotheses. 2023;14(2):66-68.
56. Ngoc VT, Ha PT, Hung DT, Anh NV. Management of clear aligner-related severe enamel demineralization with A modified resin infiltration technique: a case report. Dent Hypotheses. 2023;14(2):66-68.
57. Muhssin SA, Akram HM. Assessment of salivary levels of the RANKL and RANK in patients with healthy gingiva on reduced periodontium versus periodontitis: an analytical cross-sectional study. Dent Hypotheses. 2023;14(2):49-51.
58. Martinez-Mondragon M, Urriolagoitia-Sosa G, Romero-Ángeles B, Pérez-Partida JC, Cruz-Olivares IM, Urriolagoitia-Calderón G. Bilinear numerical analysis of the structural behavior of a dental implant applied as a biomaterial carbon fiber reinforced polyether-ether-ketone (CFR-PEEK): A finite element analysis. Dent Hypotheses. 2023;14(2):45-48.
59. Hassan DH, Al-joranii SM. Effect of feeding pattern and salivary level of growth hormone on the stage of primary tooth eruption: an analytical cross-sectional study. Dent Hypotheses. 2023;14(2), 52-54.
60. Al-hamdani GM, Yas LS. Serum and Salivary Vitamin B12 Levels among Iron Deficiency Anemia Patient with Recurrent Aphthous Stomatitis: An Analytical Cross-Sectional Study. Dent Hypotheses. 2023;14(2): 55-58.
61. Khandan A, Khosravi M, Roustazadeh D, Aghadavoudi F. Impact of alumina and carbon nanotubes on mechanical properties of a composite: molecular dynamic (MD) simulation. Iran J Chem Chem Eng. 2024.

62. Baba-Ahmadi SB, Hashemian M, Khosravi M, Khandan A. An experimental and analytical investigation of novel nanocomposite reinforced with nanoclay with enhanced properties for low velocity impact test. J Nanostruct. 2020; 10(1), 92-106.
63. Jasemi A, Moghadas BK, Khandan A, Saber-Samandari S. A porous calcium-zirconia scaffolds composed of magnetic nanoparticles for bone cancer treatment: Fabrication, characterization and FEM analysis. Ceram Int. 2022; 48(1):1314-1325.
64. Foroutan S, Hashemian M, Khandan AS. A Novel Porous Graphene Scaffold Prepared Using Freeze-Drying Technique for Orthopedic Approaches: Fabrication and Buckling Simulation Using GDQ Method. Iran J Mater Sci Eng. 2020;17(4).
65. Babaei M, Rezaei S, Khadem SS, Shirinbak I, Shabestari SB. The role of salivary C-reactive protein in systemic and oral disorders: A systematic review. Med J Islam Repub Iran. 2022;36:138.
66. Salman BN, Shabestari SB, Jam MS, Tari SA, Shirinbak I. Periodontal parameters and oral hygiene in diabetic and nondiabetic adolescents in Zanjan. Med J Islam Repub Iran. 2020;34:12.
67. Almasi S, Sabbagh MK, Barzi D, Tahooni A, Atyabi H, Shabestari SB. Relationship between clinical and laboratory findings of rheumatoid arthritis patients with their oral status and disease activity. Caspian J Intern Med. 2021;12(1):22.
68. Patil A, Banapurmath N, Hunashyal AM, Meti V, Mahale R. Development and performance analysis of novel cast AA7076-graphene amine-carbon fiber hybrid nanocomposites for structural applications. Biointerface Res Appl Chem. 2022;12(2): 1480-1489.
69. Rajendrachari S, Somashekharappa KK, Mahale RS, Vasanth S, Chikkegouda SP. A review on cyclic voltammetric investigation of toxic heavy metals. IntechOpen; 2022.
70. Mahale RS, Rajendrachari S, Vasanth S, Krishna H, Kapanigowda NS, Chikkegowda SP, Patil A. Technology and challenges in additive manufacturing of duplex stainless steels.2022.